J. Appl. Prob. Spec. Vol. **51A,** 297–309 (2014)

CELEBRATING 50 YEARS OF THE APPLIED PROBABILITY TRUST

Edited by
S. ASMUSSEN, P. JAGERS, I. MOLCHANOV and L. C. G. ROGERS

Part 7. Stochastic geometry

RETURN TO THE POISSONIAN CITY

WILFRID S. KENDALL, *University of Warwick*
Department of Statistics, University of Warwick, Coventry CV5 6FQ, UK.

APPLIED PROBABILITY TRUST
DECEMBER 2014

https://doi.org/10.1239/jap/1417528482 Published online by Cambridge University Press

RETURN TO THE POISSONIAN CITY

BY WILFRID S. KENDALL

Abstract

Consider the following random spatial network: in a large disk, construct a network using a stationary and isotropic Poisson line process of unit intensity. Connect pairs of points using the network, with initial/final segments of the connecting path formed by travelling off the network in the opposite direction to that of the destination/source. Suppose further that connections are established using 'near geodesics', constructed between pairs of points using the perimeter of the cell containing these two points and formed using only the Poisson lines not separating them. If each pair of points generates an infinitesimal amount of traffic divided equally between the two connecting near geodesics, and if the Poisson line pattern is conditioned to contain a line through the centre, then what can be said about the total flow through the centre? In Kendall (2011) it was shown that a scaled version of this flow has asymptotic distribution given by the 4-volume of a region in 4-space, constructed using an improper anisotropic Poisson line process in an infinite planar strip. Here we construct a more amenable representation in terms of two 'seminal curves' defined by the improper Poisson line process, and establish results which produce a framework for effective simulation from this distribution up to an L^1 error which tends to 0 with increasing computational effort.

Keywords: Improper anisotropic Poisson line process; mark distribution; point process; Poisson line process; Poissonian city network; Mecke–Slivnyak theorem; seminal curve; spatial network; traffic flow

2010 Mathematics Subject Classification: Primary 60D05
Secondary 90B15

1. Introduction

What can be said about flows in a random network? Aldous *et al.* [3] discussed maximum flows achievable on a complete graph with random capacities; Aldous and Bhamidi [1] considered the joint distribution of edge flows in a complete network with independent, exponentially distributed edge lengths. But what can be said about flows in a suitable random *spatial* network? In previous work with Aldous [2], it was shown that sparse Poisson line processes could be used to augment minimum-total-length networks connecting fixed sets of points in such a manner that (a) the total network length is not appreciably increased, but (b) the average network distance between two randomly chosen points exceeds the average Euclidean distance by only a logarithmic excess. This result debunks an apparently natural network efficiency statistic, but also indicates attractive features of networks formed using Poisson line processes.

The analysis in [2] used the notion of 'near geodesics' as noted in the abstract: these are paths constructed between pairs of points using the perimeter of the cell containing these two points and formed using only the Poisson lines not separating them. Follow up work in [7]

Work supported in part by the EPSRC research grant EP/K013939.

introduced the notion of a 'Poissonian city', namely a planar disk of radius n, connected by a random pattern of lines from a stationary and isotropic Poisson line process. Pairs of points in the disk are connected by near geodesics, with initial/final segments of the connecting path formed by travelling off the network in the opposite direction to that of the destination/source. Conditioning on one of the Poisson lines passing through the centre, and supposing that each pair of points in the disc generates an infinitesimal flow shared equally between two near geodesics derived from the line pattern, it can be shown that the mean flow at the centre is asymptotic to $2n^3$; moreover, the scaled flow has a distribution which converges to a proper nontrivial distributional limit [7, Section 3]. Thus, the asymptotic flow at the centre of this random spatial network is well behaved. The distribution can be realized in terms of the 4-volume of an unbounded region in $\mathbb{R}^4$ determined by an improper anisotropic Poisson line process defined on an infinite strip; however, it is a challenge to compute directly with this representation. In this paper we show how to represent the volume of this region in terms of a pair of monotonic concave curves ('seminal curves'); moreover, we establish results which demonstrate that a calculation in terms of initial segments of these seminal curves can be used to approximate the 4-volume up to an explicit L^1 error, which can be made as small as desired.

The paper is organized as follows: in Section 2 the Poissonian city and the improper line process are defined; in Section 3 we describe the representation in terms of seminal curves; in Section 4 we discuss the stochastic dynamics of a seminal curve; and in Section 5 we apply this to determine explicit L^1 error bounds. The paper concludes with Section 6, a brief discussion which mentions an open question related to exact simulation.

2. Traffic in the improper Poissonian city

A 'Poissonian city' [7] is a disk of radius n with connectivity supplied by lines from a unit-intensity stationary and isotropic Poisson line process. Recall that such a line process has intensity $\frac{1}{2}\,\mathrm{d}r\,\mathrm{d}\theta$, where the (undirected) lines are parameterized by the angle $\theta \in [0, \pi)$ and signed distance r from the origin. (The factor $\frac{1}{2}$ ensures that the number of hits on a unit segment has unit mean.) Traffic flow in the Poissonian city is supplied by so-called 'near geodesics', constructed between pairs of points using the perimeter of the cell containing these two points and formed from lines not separating them. Short Euclidean connections can be added [7, Section 1.2] so as to connect any pair of points whatsoever, whether the points lie on or off the Poisson line pattern. Conditioning on a line running through the origin $\boldsymbol{o}$, one can then study the flow through $\boldsymbol{o}$ which results if each pair of points contributes the same infinitesimal amount of flow divided equally between two alternate near geodesics [7, Section 3]. Asymptotics at $n \to \infty$ are studied using the limit obtained by considering $x \to x/n$ together with $y \to y/\sqrt{n}$: the result in the limit is an 'improper Poissonian city' formed from an improper anisotropic Poisson line process observed within an infinite strip of width 2. Coupling and symmetry arguments are used to show that the asymptotic mean flow in the centre is $2n^3$ (with limiting distribution when scaled accordingly), corresponding to a mean flow at the centre of 2 in the improper Poissonian city conditioned to have a horizontal line through $\boldsymbol{o}$ [7, Theorems 5 and 7].

In this section we give a direct description of the improper Poissonian city and its associated improper anisotropic Poisson line process, now observed in the whole plane $\mathbb{R}^2$. We first consider the intensity measure for the improper line process, using a natural choice of coordinates, namely the heights of intercepts on the two boundary lines of the infinite strip.

Definition 2.1. Consider the lines in $\mathbb{R}^2$ which are not vertical (which is to say, not parallel to the y-axis), and parameterize these lines by their intercepts $y_\pm$ on the $x = \pm 1$ axes. Denote by

https://doi.org/10.1239/jap/1417528482 Published online by Cambridge University Press

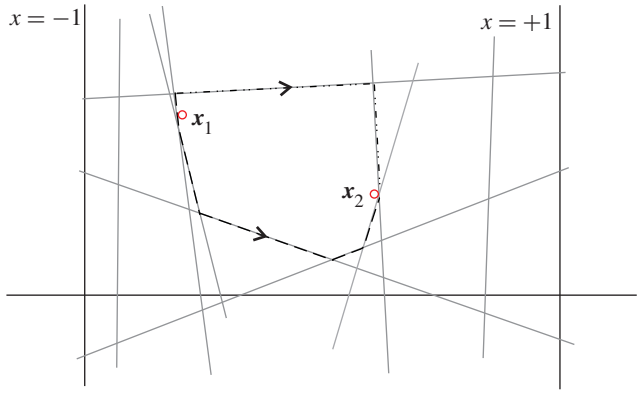

FIGURE 1: Indicative illustration of the construction of near geodesics between points $\boldsymbol{x}_1 = (x_1, y_1)$ and $\boldsymbol{x}_2 = (x_2, y_2)$ in the improper Poissonian city. The two broken lines indicate the pair of near geodesics between the two points. Necessarily, this indicative illustration omits most of the dense countably infinite set of near-vertical lines contained in Π_∞; it also omits all lines separating $\boldsymbol{x}_1$ and $\boldsymbol{x}_2$.

Π_∞ the improper anisotropic Poisson line process, composed only of nonvertical lines, whose intensity measure ν is given in the coordinates y_- and y_+ by

$$\mathrm{d}\nu = \tfrac{1}{4}\,\mathrm{d}y_-\,\mathrm{d}y_+. \tag{2.1}$$

Limiting and coupling arguments show that Π_∞ arises as the limiting line process on the infinite strip for large n if a Poissonian city within a disc of radius n is subject to inhomogeneous scaling $x \to x/n$ together with $y \to y/\sqrt{n}$. The factor $\frac{1}{4}$ arises (a) from the factor $\frac{1}{2}$ in the formula for the intensity measure of the Poisson line process of unit intensity given above, and (b) from the choice of coordinates determined by the two boundary lines of the strip, which are separated by distance 2 (contrast the expressions for ν in other coordinate systems discussed at the start of Section 4).

This line process is improper only in the sense of possessing a dense infinity of nearly vertical lines: once one removes from the line pattern all lines with absolute slope greater than a fixed constant, then the result is locally finite.

It is immediate from (2.1) that Π_∞ is statistically invariant under translations, shears along the y-axis, and reflections in the x- and y-axes. Calculations also show its statistical invariance under symmetries of the form $y \to cy$ together with $x \to c^2 x$ for $c \neq 0$ (these symmetries are exploited in [7, Section 3]).

Following [2, 7], we use Π_∞ to construct paths between distinct points $\boldsymbol{x}_1$ and $\boldsymbol{x}_2$ in $\mathbb{R}^2$ which can be thought of as 'near geodesics' in the network supplied by Π_∞, and correspond to near geodesics in the original Poissonian cities under the coupling arguments referred to above. This construction is illustrated in Figure 1.

Definition 2.2. Fix $\boldsymbol{x}_1, \boldsymbol{x}_2 \in \mathbb{R}^2$, and consider the tessellation generated by all the lines of Π_∞ which do not separate $\boldsymbol{x}_1$ and $\boldsymbol{x}_2$. Let $\mathcal{C}(\boldsymbol{x}_1, \boldsymbol{x}_2)$ be the (open) tessellation cell whose closure is the intersection of all the closed half-planes that are bounded by lines of Π_∞ and that contain both $\boldsymbol{x}_1$ and $\boldsymbol{x}_2$. The pair of *near geodesics* between $\boldsymbol{x}_1$ and $\boldsymbol{x}_2$ is given by the two connected components obtained by removing $\boldsymbol{x}_1$ and $\boldsymbol{x}_2$ from the perimeter $\partial\mathcal{C}(\boldsymbol{x}_1, \boldsymbol{x}_2)$.

In contrast to the case of [2, 7] (where initial/final segments of the connecting path have to be formed *off* the Poisson line process, by travelling in the opposite direction to that of

https://doi.org/10.1239/jap/1417528482 Published online by Cambridge University Press

the destination/source), the points $\boldsymbol{x}_1$ and $\boldsymbol{x}_2$ belong to the closed set $\partial\mathcal{C}(\boldsymbol{x}_1, \boldsymbol{x}_2)$, since there are infinitely many nearly vertical lines arbitrarily close to $\boldsymbol{x}_1$ (respectively, $\boldsymbol{x}_2$) which do not separate $\boldsymbol{x}_1$ and $\boldsymbol{x}_2$.

We use these near geodesics to define a flow over the whole plane $\mathbb{R}^2$: the infinitesimal flow between $\boldsymbol{x}_1$ and $\boldsymbol{x}_2$ amounts to the infinitesimal quantity $\mathrm{d}\boldsymbol{x}_1\,\mathrm{d}\boldsymbol{x}_2$, and this is divided equally between the two near geodesics between $\boldsymbol{x}_1$ and $\boldsymbol{x}_2$. We focus attention on the total amount of flow passing through the origin $\boldsymbol{o}$ that is produced by pairs of points lying on the infinite vertical strip $\{\boldsymbol{x} = (x, y)\colon -1 < x < 1\}$, when we condition on there being a horizontal line $\ell^* \in \Pi_\infty$ which passes through $\boldsymbol{o}$ (so in fact ℓ^* is the x-axis). Under this conditioning, the total flow of interest is given by

$$T = \int_{-\infty}^{\infty}\int_{-1}^{+1}\int_{-\infty}^{\infty}\int_{-1}^{x_2} \frac{1}{2}\,\mathbf{1}_{[\boldsymbol{o}\in\partial\mathcal{C}((x_1,y_1),(x_2,y_2))]}\,\mathrm{d}x_1\,\mathrm{d}y_1\,\mathrm{d}x_2\,\mathrm{d}y_2. \tag{2.2}$$

Here the factor $\frac{1}{2}$ allows for the splitting of the flow between the two possible near geodesics. Note for future use the Slivynak–Mecke theorem [5, Example 4.3]: if Π_∞ is so conditioned then $\Pi_\infty \setminus \{\ell^*\}$ is distributed as the original unconditioned improper anisotropic Poisson line process. So, from henceforth, the construction of near geodesics, as in Definition 2.2, is based on $\Pi_\infty \cup \{\ell^*\}$ rather than Π_∞.

An interaction between the improper nature of Π_∞ and its statistical symmetries can be used to somewhat simplify the quantity (2.2). If one of $\boldsymbol{x}_1$ or $\boldsymbol{x}_2$ lies in the open upper half-plane and the other lies in the open lower half-plane, then the perimeter $\partial\mathcal{C}(\boldsymbol{x}_1, \boldsymbol{x}_2)$ of the (convex) cell will almost surely (in $\boldsymbol{x}_1$ and $\boldsymbol{x}_2$) not contain $\boldsymbol{o}$. This is a consequence of the horizontal translation symmetry of the statistics of $\Pi_\infty \cup \{\ell^*\}$. Accordingly, we can divide the multiple integral (2.2) into two nonzero and identically distributed parts, integrating respectively over $y_1 > 0$ and $y_2 > 0$, and $y_1 < 0$ and $y_2 < 0$. We shall see in the next section that the contributions from these two parts are independent.

Suppose that $\boldsymbol{x}_1$ and $\boldsymbol{x}_2$ both lie in the open right-hand half of the open upper half-plane, namely, $\{(x, y)\colon x > 0,\ y > 0\}$. Since the improper line process Π_∞ contains infinitely many arbitrarily steep lines with x-intercepts dense on the x-axis, it follows that the near geodesics between such $\boldsymbol{x}_1$ and $\boldsymbol{x}_2$ cannot pass through $\boldsymbol{o}$, and so such configurations cannot contribute to (2.2). Similarly, no contribution can be made from configurations in which $\boldsymbol{x}_1$ and $\boldsymbol{x}_2$ both lie in the left-hand half of the upper half-plane, namely, $\{(x, y)\colon x < 0,\ y > 0\}$.

Accordingly, the properties of (2.2) will follow from analysis of

$$F = \int_{Q_+}\int_{Q_-} \frac{1}{2}\,\mathbf{1}_{[\boldsymbol{o}\in\partial\mathcal{C}(\boldsymbol{x}_1,\boldsymbol{x}_2)]}\,\mathrm{d}\boldsymbol{x}_1\,\mathrm{d}\boldsymbol{x}_2, \tag{2.3}$$

where $Q_+ = \{(x, y)\colon 0 < x < 1,\ y > 0\}$ and $Q_- = \{(x, y)\colon -1 < x < 0,\ y > 0\}$. In fact the quantity in (2.2) will be the independent sum of two copies of F, one for the upper and one for the lower half-planes. In [7] this representation is used to establish some general properties of the flow at the centre. However, it is desirable to construct a representation of F more amenable to quantitative arguments and effective approximation. We will now show how to do this.

3. Separation and seminal curves

We focus on the upper half-plane case, and the 4-volume $2F$ of the subset $\mathcal{D}^{\mathrm{upper}} \subset Q_- \times Q_+$ given by

$$\mathcal{D}^{\mathrm{upper}} = \{(\boldsymbol{x}_1, \boldsymbol{x}_2) \in Q_- \times Q_+\colon\ \boldsymbol{o} \in \partial\mathcal{C}(\boldsymbol{x}_1, \boldsymbol{x}_2)\}.$$

https://doi.org/10.1239/jap/1417528482 Published online by Cambridge University Press

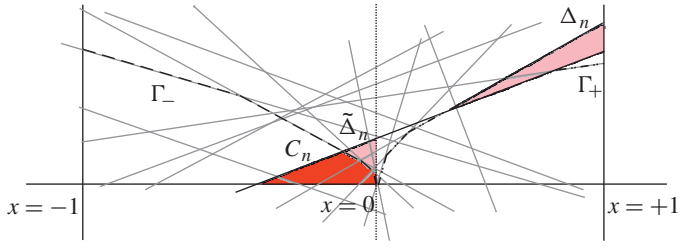

FIGURE 2: The two seminal curves Γ_- and Γ_+, and the regions $\Delta_n = \Delta_n^+$, $C_n = C_n^+$, and $\widetilde{\Delta}_n = \widetilde{\Delta}_n^+$. Note that Δ_n and $\widetilde{\Delta}_n$ are triangular regions determined using only lines that are components of Γ_+, the x-axis, and the $x = 1$ axis. The region C_n is contained in the triangular region $\widetilde{\Delta}_n$, and uses lines that are components either of Γ_+ or of Γ_-, as well as the x-axis. Note that in fact $\Gamma_\pm$ have vertical asymptotes at 0.

Thus, $\mathcal{D}^{\text{upper}}$ is composed of point pairs $(\boldsymbol{x}_1, \boldsymbol{x}_2) \in Q_- \times Q_+$ such that the line segment connecting $\boldsymbol{x}_1$ with $\boldsymbol{x}_2$ is not separated from $\boldsymbol{o}$ by Π_∞. Note that such separation fails if and only if no one line $\ell \in \Pi_\infty$ simultaneously separates $\boldsymbol{x}_1$ and $\boldsymbol{x}_2$ from $\boldsymbol{o}$.

Consider a dual construction, using the lines of Π_∞, that builds sets of lines of positive and negative slopes which could in principle separate the origin $\boldsymbol{o}$ and some line segment between some $\boldsymbol{x}_1 \in Q_-$ and some $\boldsymbol{x}_2 \in Q_+$:

$$\Pi_{\infty,+} = \{\ell \in \Pi_\infty : \ell \text{ has positive slope, } \ell \text{ intercepts the negative } x\text{-axis}\},$$
$$\Pi_{\infty,-} = \{\ell \in \Pi_\infty : \ell \text{ has negative slope, } \ell \text{ intercepts the positive } x\text{-axis}\}.$$

The lines relevant to the case of $\boldsymbol{x}_1$ and $\boldsymbol{x}_2$ lying in the lower half-plane lie in $\Pi_\infty \setminus (\Pi_{\infty,-} \cup \Pi_{\infty,+})$; hence (as mentioned in Section 2), the total flow (2.2) is indeed the sum of two independent copies of the upper half-plane contribution $2F$, for F as specified in (2.3).

Now define the *seminal curves* $\Gamma_\pm$ as the concave lower envelopes of the unions of lines in $\Pi_{\infty,\pm}$: for $s \in (0, 1]$,

$$\Gamma_-(-s) = \inf\{\text{height of intercept of } \ell \text{ on } x = -s : \ell \in \Pi_{\infty,-}\}, \tag{3.1}$$
$$\Gamma_+(s) = \inf\{\text{height of intercept of } \ell \text{ on } x = s : \ell \in \Pi_{\infty,+}\}. \tag{3.2}$$

These curves are illustrated in Figure 2. It is immediate that both curves are concave and continuous, and that Γ_- is strictly monotonically decreasing and Γ_+ is strictly monotonically increasing. Therefore, the inverses $\Gamma_-^{-1}(\varepsilon)$ and $\Gamma_+^{-1}(\varepsilon)$ are well defined for $0 < \varepsilon \le \Gamma_-(-1)$ and $0 < \varepsilon \le \Gamma_+(1)$, respectively: it is convenient to adopt the convention that $\Gamma_\pm^{-1}(\varepsilon) = \pm 1$ for $\varepsilon > \Gamma_\pm(\pm 1)$.

A simple lower bound for the quantity (2.3) arises from the observation that

$$\{(x, y) \in Q_- : 0 < y < \Gamma_-(x)\} \times \{(x, y) \in Q_+ : 0 < y < \Gamma_+(x)\} \subset \mathcal{D}^{\text{upper}}. \tag{3.3}$$

From this inclusion relation we deduce that

$$\int_{-1}^{0} \Gamma_-(s)\,\mathrm{d}s \int_{0}^{1} \Gamma_+(s)\,\mathrm{d}s < \text{Leb}_4(\mathcal{D}^{\text{upper}}) = 2F. \tag{3.4}$$

Evidently, it is feasible to approximate both $\int_{-1}^{0} \Gamma_-(s)\,\mathrm{d}s$ and $\int_0^1 \Gamma_+(s)\,\mathrm{d}s$ to within an additive absolute error of $\varepsilon > 0$ using only finitely many lines from Π_∞, namely the lines involved in the initial segments $\{\Gamma_-(s) : -1 \le s \le \Gamma_-^{-1}(\varepsilon)\}$ and $\{\Gamma_+(s) : \Gamma_-^{-1}(\varepsilon)) \le s \le 1\}$. We will see in Section 5 how this leads to an effective approximation.

https://doi.org/10.1239/jap/1417528482 Published online by Cambridge University Press

We therefore turn attention to the difference between the two sides of (3.4), or, equivalently, the 4-volume of the difference between the two regions in (3.3). The difference region splits into two disjoint parts whose definitions are related by the mirror symmetry around the y-axis. First observe that if $\boldsymbol{x}_1 = (x_1, y_1) \in Q_-$ lies above Γ_-, and $\boldsymbol{x}_2 \in Q_+$ lies above Γ_+, then the line segment connecting $\boldsymbol{x}_1$ with $\boldsymbol{x}_2$ is separated from $\boldsymbol{o}$. Indeed, we can use any line realizing the infimum in the definition of $\Gamma_-(x_1)$ (or any analogous line realizing the infimum in the definition of $\Gamma_+(x_2)$). So we can focus on the case when $\boldsymbol{x}_2 = (x_2, y_2)$ lies above Γ_+ while $\boldsymbol{x}_1 = (x_1, y_1)$ lies below Γ_-, and use mirror symmetry to deal with the opposite case. Consider the lines $\ell_0, \ell_1, \ell_2, \ldots$ of $\Pi_{\infty,+}$ which are components of $\{\Gamma_+(s)\colon 0 < s \le 1\}$, enumerated according to the increasing heights of their intercepts on $x = 1$. Then $\boldsymbol{o} \in \partial\mathcal{C}(\boldsymbol{x}_1, \boldsymbol{x}_2)$ if and only if any ℓ_n lying below $\boldsymbol{x}_2$ has to pass above $\boldsymbol{x}_1$. As a consequence of the infimum-based definition (3.2) of Γ_+ and of the concavity of Γ_+, ℓ_{n+1} must intersect ℓ_n, and it must do so at a larger x-coordinate than where it intersects Γ_+. Using concavity and monotonicity of Γ_+, it may be deduced that the intercept of ℓ_n on the $x = x_1 < 0$ axis must be decreasing in n. Let $n(\boldsymbol{x}_2)$ be the largest n such that ℓ_n lies below $\boldsymbol{x}_2$; then the set $C^+_{n(\boldsymbol{x}_2)}$ of $\boldsymbol{x}_1$ with $\boldsymbol{o} \in \partial\mathcal{C}(\boldsymbol{x}_1, \boldsymbol{x}_2)$ is exactly the set of those points in Q_- which lie below Γ_- and also below $\ell_{n(\boldsymbol{x}_2)}$. Let Δ^+_n be the triangle formed by ℓ_n, ℓ_{n+1}, and the $x = 1$ axis. These regions are illustrated in Figure 2, as well as the further region $\widetilde{\Delta}^+_n$ to be defined below.

Let C^-_n and Δ^-_n be the analogous regions for lines that are components of Γ_-. Evidently, the areas of both C^-_n and C^+_n for any fixed n can be approximated to within an additive absolute error of $\varepsilon > 0$, using only the lines involved in $\{\Gamma_-(s)\colon -1 \le s \le \Gamma_-^{-1}(\varepsilon)\}$ and $\{\Gamma_+(s)\colon \Gamma_-^{-1}(\varepsilon) \le s \le 1\}$, and the same is trivially true of the triangles $\Delta^\pm_n$.

It now follows that we can represent F in (2.3) in a way that lends itself to an effective approximation so long as we have a useful representation of the curves $\Gamma_\pm$ viewed as continuous piecewise-linear random processes; we summarize this in the following theorem.

Theorem 3.1. *Given the analysis below of $\Gamma_\pm$ as continuous piecewise-linear random processes,*

$$\begin{aligned} 2F &= \int_{Q_+}\int_{Q_-} \mathbf{1}_{[\boldsymbol{o}\in\partial\mathcal{C}(\boldsymbol{x}_1,\boldsymbol{x}_2)]}\,\mathrm{d}\boldsymbol{x}_1\,\mathrm{d}\boldsymbol{x}_2 \\ &= \int_0^1 \Gamma_-(-s)\,\mathrm{d}s \int_0^1 \Gamma_+(t)\,\mathrm{d}t + \sum_{n=0}^{\infty} \mathrm{Leb}_2(C^+_n)\,\mathrm{Leb}_2(\Delta^+_n) + \sum_{n=0}^{\infty} \mathrm{Leb}_2(C^-_n)\,\mathrm{Leb}_2(\Delta^-_n) \end{aligned} \tag{3.5}$$

enables an effective computation of the left-hand side $2F$; indeed, finite truncations of the convergent infinite sums use calculations based on only finitely many of the lines involved in the constructions of $\Gamma_\pm$.

Proof. Using the calculations of [7, Section 3], we can deduce that $\mathbb{E}[F] < \infty$ and, therefore, that the infinite sums of nonnegative terms on the right-hand side are convergent. By the above arguments, given the subsequent stochastic analysis of $\Gamma_\pm$, we may then approximate $\int_0^1 \Gamma_-(-s)\,\mathrm{d}s$ to within an additive absolute error of $\sqrt{\varepsilon/2}/\Gamma_+(1)$ and $\int_0^1 \Gamma_+(t)\,\mathrm{d}t$ to within an additive absolute error of $\sqrt{\varepsilon/2}/\Gamma_-(-1)$. Since $\int_0^1 \Gamma_-(-s)\,\mathrm{d}s < \Gamma_-(-1)$ and $\int_0^1 \Gamma_+(t)\,\mathrm{d}t < \Gamma_+(1)$, it follows that the product of integrals on the right-hand side of (3.5) can be approximated to within an additive absolute error of $\varepsilon/2$. Moreover, we can choose to approximate each term $\mathrm{Leb}_2(C^\pm_n)$ in the two infinite sums to within an additive absolute error of $2^{-n-2}\varepsilon/\mathrm{Leb}_2(\Delta^\pm_n)$. Accordingly, the entire expression can be approximated to within an additive absolute error of ε. While this approximation uses all of $\Gamma_\pm$, we may truncate the absolutely convergent sums

https://doi.org/10.1239/jap/1417528482 Published online by Cambridge University Press

as required to produce an approximation of any required accuracy using only finitely many of these lines.

In the remainder of this paper we improve on this result by showing that we can provide an explicit L^1-approximation, by bounding the mean tails of the infinite sums in (3.5). To prepare for this, consider the region C_n^+. We can produce a simple triangular approximation region as follows: for each $n \geq 0$, let $\widetilde{\Delta}_n^+$ be the triangle formed by ℓ_n, the x-axis, and the $x = 0$ axis; note that this region contains C_n^+. Again, this region is illustrated in Figure 2. We can then replace the regions involved in the tails of the infinite sums in (3.5). For example,

$$\bigcup_{n=N}^{\infty} (C_n^+ \times \Delta_n^+) \subseteq \bigcup_{n=N}^{\infty} (\widetilde{\Delta}_n^+ \times \Delta_n^+). \tag{3.6}$$

Note that the approximating sets $\widetilde{\Delta}_n^+$ are now formed entirely from lines in $\Pi_{\infty,+}$. A similar argument applies for the sum involving C_n^- rather than C_n^+, resulting in an approximating tail using regions formed entirely from lines in $\Pi_{\infty,-}$, and, therefore, the two corrections are independent. If we can obtain *a priori* bounds for the two correction regions then we have an effective truncated approximation for (3.5), namely,

$$\int_0^1 \Gamma_-(-s)\,\mathrm{d}s \int_0^1 \Gamma_+(t)\,\mathrm{d}t + \sum_{n=0}^{N} \mathrm{Leb}_2(C_n^+)\,\mathrm{Leb}_2(\Delta_n^+) + \sum_{n=0}^{N} \mathrm{Leb}_2(C_n^-)\,\mathrm{Leb}_2(\Delta_n^-). \tag{3.7}$$

This truncated approximation can then itself be approximated in finitary terms, in the sense of involving the use of only a finite number of lines of Π_∞ obtained from $\{\Gamma_-(s)\colon -1 \leq s \leq 1/m_-\}$ and $\{\Gamma_+(s)\colon 1/m_+ \leq s \leq 1\}$ for suitable $m_\pm$.

To complete our analysis of the 4-volume specified in (3.6), we now need to determine the dynamics of the random processes $\{\Gamma_\pm(s)\colon s \in (0, 1]\}$, both to show that the computations involved in the representation given by Theorem 3.1 can be achieved effectively, and to obtain explicit control of the mean behaviour of the tails of the infinite sums using the upper bounds

$$\sum_{n=N}^{\infty} \mathrm{Leb}_2(\widetilde{\Delta}_n^+)\,\mathrm{Leb}_2(\Delta_n^+). \tag{3.8}$$

4. Seminal curve dynamics

To prepare for the calculation of the seminal curve dynamics, we first compute expressions for the intensity measure ν in two different coordinate frames. Consider first the coordinates arising from intercepts y_0 and y_s on $x = 0$ and $x = s$ for some fixed $s > 0$. This is a linear transformation of coordinates, resulting in

$$\mathrm{d}\nu = \frac{\mathrm{d}y_0\,\mathrm{d}y_s}{2s}. \tag{4.1}$$

Equation (4.1) makes it evident that ν and, thus, Π_∞ satisfy the (statistical) symmetry $y \to cy$, $x \to c^2 x$ for nonzero c. Now consider new coordinates given by slope σ and intersection x with a fixed reference line of slope σ_0, and intercepts b_0 and b_s on $x = 0$ and $x = s$ for some fixed $s > 0$. In y_0, y_s coordinates we find that

$$(s - x)b_0 + xb_s = (s - x)y_0 + xy_s, \qquad y_0 + \sigma x = b_0 + \sigma_0 x.$$

Now examine $\nu_{\infty,+}$ obtained as the intensity measure of $\Pi_{\infty,+}$. We obtain different answers for the regions in which σ is less than or greater than σ_0; recalling that all lines in $\Pi_{\infty,+}$ are of

https://doi.org/10.1239/jap/1417528482 Published online by Cambridge University Press

positive slope and intersect the negative part of the x-axis, calculations yield

$$\mathrm{d}\nu_{\infty,+} = \tfrac{1}{2}(\sigma_0 - \sigma)\,\mathrm{d}\sigma\,\mathrm{d}x \quad \text{for } 0 < \sigma < \sigma_0, \tag{4.2}$$

$$\mathrm{d}\nu_{\infty,+} = \tfrac{1}{2}(\sigma - \sigma_0)\,\mathrm{d}\sigma\,\mathrm{d}x \quad \text{for } \sigma_0 < \sigma < \sigma_0 + b_0/x. \tag{4.3}$$

For convenience, we focus on the $\Gamma = \Gamma_+$ case. We now calculate the one-point joint distribution of $(\Gamma(s), \Gamma'(s))$ for $0 < s \le 1$, bearing in mind that the two-sided derivative $\Gamma'(s)$ exists only almost surely for each fixed nonzero s.

Lemma 4.1. *For $s \in (0, 1]$,*

$$\mathbb{P}\{\Gamma(s) > \gamma\} = \mathrm{e}^{-\gamma^2/(4s)} \quad \textit{for } \gamma > 0, \tag{4.4}$$

$$\mathcal{L}(\Gamma'(s)) = \mathrm{Uniform}\left[0, \frac{\Gamma(s)}{s}\right].$$

In particular, $\Gamma(s)$ has a Rayleigh$(\sqrt{2s}\,)$ distribution.

Proof. Consider the intensity measure ν in y_0, y_s coordinates, as specified in (4.1). It follows that the point process of intersections of the $x = s$ axis with lines from $\Pi_{\infty,+}$, with each intersection marked by the slope of the corresponding line, is given by an inhomogeneous Poisson process of points $0 < t_1 < t_2 < \cdots$, with intensity measure $(t/2s)\,\mathrm{d}t$, such that each point t_m is independently marked by a slope with distribution Uniform$[0, t_m/s]$. The result follows immediately.

These arguments can be extended to determine the two-point joint distribution of the pair of pairs $(\Gamma(s), \Gamma'(s))$ and $(\Gamma(t), \Gamma'(t))$. However, for the purposes of Theorem 3.1, we need to understand the dynamical behaviour of the random process $\{\Gamma(s) : s \in (0, 1]\}$. It turns out to be most convenient to study this process in reversed time, so we take $\Gamma'(s)$ to be continuous from the left and to have right limits ('càglàd', in the common French probabilistic terminology).

Theorem 4.1. *Let the times of changes in the slope of $\{\Gamma(s) : 0 < s \le 1\}$ in reversed time be*

$$1 = S_0 > S_1 > S_2 > \cdots > 0.$$

Then the tangent lines $\ell_0, \ell_1, \ell_2, \ldots$, enumerated as in Section 3, have respective slopes $\Gamma'(s)$ for $S_n \ge s > S_{n+1}$. With $Y_n = \Gamma(S_n) - S_n\Gamma'(S_n)$ denoting the intercept of ℓ_n on the y-axis, $(S_{n+1}, \Gamma'(S_{n+1}))$ is expressible as

$$\frac{1}{S_{n+1}} = \frac{1}{S_n} + \frac{4}{Y_n^2} E_{n+1}, \tag{4.5}$$

$$\Gamma'(S_{n+1}) = \Gamma'(S_n) + \frac{Y_n}{S_{n+1}}\sqrt{U_{n+1}}, \tag{4.6}$$

where each E_n has the standard exponential distribution and U_n the Uniform$[0, 1]$ distribution, all $\{E_n\}$ and $\{U_n\}$ are independent of each other and of $\Gamma(S_0) = \Gamma(1)$ and $\Gamma'(S_0) = \Gamma'(1)$, and $(\Gamma(S_0), \Gamma'(S_0))$ has the joint distribution given in Lemma 4.1.

This yields a dynamical algorithm to simulate $\Gamma(s)$ segment-by-segment as s decreases to 0. This is what is required in order to generate a simulation recipe for approximation (3.7).

Proof of Theorem 4.1. Again, the proof follows from re-expressing the intensity measure ν in new coordinates, this time as given by (4.3). This calculation can be applied to the point process of intersections of $\Pi_{\infty,+}$ with a fixed reference line of slope σ_0, and intercepts b_0 and b_s on $x = 0$ and $x = s$ for some fixed $s > 0$. Restrict attention to the case when the

https://doi.org/10.1239/jap/1417528482 Published online by Cambridge University Press

intercepting line has slope greater than σ_0. Considering the point process of intercepts with each intersection marked by the slope of the corresponding line, the subprocess of intercepts $0 < x_1 < x_2 < \cdots$ with slope greater than σ_0 has intensity measure $\frac{1}{4}(b_0/x)^2\,\mathrm{d}x$, and each point x_m is independently marked by a slope with density $2(\sigma - \sigma_0)/(b_0/x)^2$ for $0 < \sigma_0 < \sigma < \sigma_0 + b_0/x$. The result follows by calculation.

These dynamics are 'reverse-time dynamics'. The calculations of (4.2) could be applied to determine 'forward-time dynamics'; however, these are not useful for our current purposes.

We now state and prove three corollaries about the behaviour of the system $\{(S_n, Y_n) : n \geq 0\}$. The recursive system (4.5) and (4.6) leads to a delightfully simple expression for the intercept process $\{Y_n : n \geq 0\}$ as a perpetuity [11].

Corollary 4.1. *In the notation of Theorem 4.1,*

$$Y_{n+1} = Y_n(1 - \sqrt{U_{n+1}}) = Y_0 \prod_{m=1}^{n+1} (1 - \sqrt{U_m}). \tag{4.7}$$

In particular, $\limsup_{n\to\infty} 3^n Y_n$ *is a finite random variable, so that, almost surely,* Y_n *converges to* 0 *geometrically fast.*

Proof. The perpetuity equation (4.7) can be deduced directly from the expression for Y_n and (4.6). It follows from $\mathbb{E}[1 - \sqrt{U_n}\,] = \frac{1}{3}$ that $\{3^n Y_n : n \geq 0\}$ is a nonnegative martingale, and, therefore, converges to a nonnegative random limit.

From (4.5) we can deduce that

$$\frac{Y_{n+1}^2}{S_{n+1}} = \frac{Y_{n+1}^2}{S_n} + 4\frac{Y_{n+1}^2}{Y_n^2}E_{n+1} = \frac{Y_{n+1}^2}{Y_n^2}\left(\frac{Y_n^2}{S_n} + 4E_{n+1}\right) = (1 - \sqrt{U_{n+1}})^2\left(\frac{Y_n^2}{S_n} + 4E_{n+1}\right).$$

Consequently, we can take conditional expectations, and use independence and a Foster–Lyapunov argument (see [8, Chapter 15, especially Theorem 15.0.1] or [10, Theorem 3.1]) to reveal the following.

Corollary 4.2. $\{Y_n^2/S_n : n \geq 0\}$ *forms a geometrically ergodic Markov chain.*

One further step is useful in understanding the error bound.

Corollary 4.3. $\{\mathbb{E}[Y_n^3/S_n]\}$ *converges to* 0 *geometrically fast. Indeed,*

$$\mathbb{E}\left[\frac{Y_n^3}{S_n}\right] \leq (\text{constant})\,3^{-n}$$

and $\{Y_n^3/S_n\}$ *almost surely converges to* 0 *geometrically fast.*

Proof. Applying (4.5),

$$\begin{aligned}
\mathbb{E}\left[3^n\frac{Y_n^3}{S_n}\right] &= \mathbb{E}\left[3^n\frac{Y_n^3}{Y_{n-1}^3}\left(\frac{Y_{n-1}^3}{S_{n-1}} + 4Y_{n-1}E_n\right)\right] \\
&= \mathbb{E}\left[3^n(1 - \sqrt{U_n})^3\left(\frac{Y_{n-1}^3}{S_{n-1}} + 4Y_{n-1}E_n\right)\right] \\
&= \frac{3}{10}\mathbb{E}\left[3^{n-1}\frac{Y_{n-1}^3}{S_{n-1}} + 4Y_0\right]
\end{aligned}$$

https://doi.org/10.1239/jap/1417528482 Published online by Cambridge University Press

$$= \mathbb{E}\left[\left(\frac{3}{10}\right)^n \frac{Y_0^3}{S_0} + 4\left(\left(\frac{3}{10}\right)^n + \left(\frac{3}{10}\right)^{n-1} + \cdots + \frac{3}{10}\right) Y_0\right]$$
$$\leq \mathbb{E}\left[\left(\frac{3}{10}\right)^n \frac{Y_0^3}{S_0} + \frac{12}{7} Y_0\right].$$

But $S_0 = 1$ while Y_0 has a Rayleigh($\sqrt{2}$) distribution and, therefore, has finite moments of all orders.

5. Flow in the centre of the city

From the above work, we can represent the flow at the centre of the city in terms of the seminal curves. Here we establish an explicit upper bound on the L^1 error that arises if we use only finite portions of the seminal curves.

Consider the tail sum (3.8), from which we can obtain an L^1 upper bound on the error term. This can be expressed in terms of the quantities studied in the dynamical system given by (4.5) and (4.6). That is,

$$\sum_{n=N}^{\infty} \mathrm{Leb}_2(\widetilde{\Delta}_n^+)\, \mathrm{Leb}_2(\Delta_n^+) = \frac{1}{4} \sum_{n=N}^{\infty} (1 - S_{n+1})^2\, Y_n^2 \left(\frac{\Gamma'(S_{n+1})}{\Gamma'(S_n)} - 1\right)$$

since

$$\mathrm{Leb}_2(\widetilde{\Delta}_n^+) = \frac{1}{2} Y_n \times \frac{Y_n}{\Gamma'(S_n)},$$
$$\mathrm{Leb}_2(\Delta_n^+) = \tfrac{1}{2}(1 - S_{n+1}) \times (\Gamma'(S_{n+1}) - \Gamma'(S_n))(1 - S_{n+1}).$$

We now estimate the nth summand of (3.8) for any $n \geq N$, using the fact that $0 < S_n \leq 1$, the above details about the stochastic dynamics, and the fact that Γ' is monotonically decreasing. Using (4.5) and (4.6),

$$(1 - S_{n+1})^2 Y_n^2 \left(\frac{\Gamma'(S_{n+1})}{\Gamma'(S_n)} - 1\right)$$
$$\leq Y_n^2 \left(\frac{\Gamma'(S_{n+1})}{\Gamma'(S_n)} - 1\right)$$
$$= Y_n^3 \left(\frac{\sqrt{U_{n+1}}}{\Gamma'(S_n) S_{n+1}}\right)$$
$$= \frac{Y_n^3 \sqrt{U_{n+1}}}{\Gamma'(S_n)} \left(\frac{4}{Y_n^2} E_{n+1} + \frac{4}{Y_{n-1}^2} E_n + \cdots + \frac{4}{Y_N^2} E_{N+1} + \frac{1}{S_N}\right)$$
$$\leq \frac{4 Y_n \sqrt{U_{n+1}}}{\Gamma'(S_N)} \left[E_{n+1} + \left(\frac{Y_n}{Y_{n-1}}\right)^2 E_n + \cdots + \left(\frac{Y_n}{Y_N}\right)^2 E_{N+1}\right] + \frac{Y_n^3 \sqrt{U_{n+1}}}{\Gamma'(S_N) S_N}.$$

Now take conditional expectations given $\Gamma'(S_N)$, S_N, and Y_N, and use the independence of E_n and Y_n / Y_N (for $n \geq N$) to convert the conditional expectations into absolute expectations, using also the product expression (4.7) for the perpetuity Y_n and the fact that $\Gamma'(S_N) \geq \Gamma'(S_0)$ for $N \geq 0$:

$$\mathbb{E}\left[(1 - S_{n+1})^2 Y_n^2 \left(\frac{\Gamma'(S_{n+1})}{\Gamma'(S_n)} - 1\right) \,\middle|\, \Gamma'(S_N), S_N, Y_N\right]$$
$$\leq \frac{2}{3} \frac{Y_N}{\Gamma'(S_N)} \left\{4\, \mathbb{E}\left[\frac{Y_n}{Y_N}\left(1 + \left(\frac{Y_n}{Y_{n-1}}\right)^2 + \cdots + \left(\frac{Y_n}{Y_N}\right)^2\right)\right] + \mathbb{E}\left[\left(\frac{Y_n}{Y_N}\right)^3\right] \frac{Y_N^2}{S_N}\right\}$$

https://doi.org/10.1239/jap/1417528482 Published online by Cambridge University Press

$$\le \frac{2}{3}\frac{Y_N}{\Gamma'(S_N)}\left\{4\left[1+\frac{3}{10}+\cdots+\left(\frac{3}{10}\right)^{n-N}\right]\left(\frac{1}{3}\right)^{n-N}+\left(\frac{1}{10}\right)^{n-N}\frac{Y_N^2}{S_N}\right\}$$
$$\le \frac{2}{3}\frac{Y_N}{\Gamma'(S_N)}\left[\frac{40}{7}\left(\frac{1}{3}\right)^{n-N}+\frac{Y_N^2}{S_N}\left(\frac{1}{10}\right)^{n-N}\right].$$

Hence,

$$\mathbb{E}\left[\sum_{n=N}^{\infty}\mathrm{Leb}_2(\widetilde{\Delta}_n^+)\,\mathrm{Leb}_2(\Delta_n^+)\;\middle|\;\Gamma'(S_N),S_N,Y_N\right]\le\frac{5}{\Gamma'(S_N)}\left(\frac{2}{7}Y_N+\frac{1}{27}\frac{Y_N^3}{S_N}\right)\tag{5.1}$$
$$\le\frac{5}{\Gamma'(S_0)}\left(\frac{2}{7}Y_N+\frac{1}{27}\frac{Y_N^3}{S_N}\right).\tag{5.2}$$

Now Y_N and Y_N^3/S_N almost surely converge geometrically fast to 0 (use Corollaries 4.1 and 4.3). Hence, almost surely, the above conditional expectation tends to 0 as $N\to\infty$. Moreover, we have the following explicit L^1 error bound, converging geometrically fast to 0 with N.

Theorem 5.1. *The L^1 error of the approximation at (3.7) for the quantity $2F$ at (3.5) is bounded above by*

$$\frac{20}{7}\times 3^{-N}+\frac{20}{27}\times 6^{-N}.$$

Proof. By our previous work, notably (5.2), we can obtain a bound on the approximation error for (3.7) by replacing N by $N-1$ in the sum of (a) the term

$$\frac{5}{\Gamma'(S_N)}\left(\frac{2}{7}Y_N+\frac{1}{27}\frac{{Y_N}^3}{S_N}\right)$$

from the right-hand side of (5.1), and (b) the corresponding term for the left seminal curve Γ_- as opposed to $\Gamma_+=\Gamma$. We now estimate the quantity in (a).

First, observe that (4.6), and the fact that $Y_0\le\Gamma(1)$, allows us to deduce that

$$\mathbb{E}\left[\frac{Y_N^3}{\Gamma'(S_N)S_N}\right]\le\mathbb{E}\left[\frac{Y_N^3}{Y_{N-1}\sqrt{U_N}}\right]$$
$$=\mathbb{E}\left[\frac{(1-\sqrt{U_N})^3}{\sqrt{U_N}}\right](\mathbb{E}[(1-\sqrt{U_1})^2])^{N-1}\,\mathbb{E}[Y_0^2]$$
$$\le\tfrac{1}{2}\times 6^{-(N-1)}\,\mathbb{E}[\Gamma(1)^2]$$
$$=2\times 6^{-(N-1)},$$

where in the last step we used the fact that $\Gamma(1)$ has a Rayleigh($\sqrt{2}$) distribution; see (4.4). Second, consider

$$\mathbb{E}\left[\frac{Y_N}{\Gamma'(S_N)}\right]\le\mathbb{E}\left[\frac{Y_N}{\Gamma'(S_1)}\right]$$
$$\le\mathbb{E}\left[\frac{Y_NS_1}{Y_0\sqrt{U_1}}\right]$$
$$\le\mathbb{E}\left[\frac{Y_N}{Y_0\sqrt{U_1}}\right]$$
$$=(\mathbb{E}[1-\sqrt{U_2}\,])^{N-1}\,\mathbb{E}\left[\frac{1-\sqrt{U_1}}{\sqrt{U_1}}\right]$$
$$=3^{-(N-1)}.$$

https://doi.org/10.1239/jap/1417528482 Published online by Cambridge University Press

The result follows by calculating the contribution from (a) and then doubling to account for the contribution from (b).

A variation on this argument gives a geometrically decaying *conditional* L^1 error bound given S_N, Y_N, and $\Gamma'(S_N)$, and their counterparts for the left seminal curve Γ_- as opposed to Γ_+. However, this conditional L^1 error bound is rather inelegant, since the quantities $C_n^{\pm}$ in (3.7) depend on S_m, Y_m, and $\Gamma'(S_m)$ for $m \geq N$.

We can summarize these results as follows: the 4-volume given by (2.2) can be approximated to any desired accuracy in L^1, based on the construction of initial segments of the seminal curves $\{\Gamma_-(s)\colon -1 \leq s \leq 1/m_-\}$ and $\{\Gamma_+(s)\colon 1/m_+ \leq s \leq 1\}$, and their lower half-plane counterparts, for suitable $m_\pm$, using Theorem 3.1, Lemma 4.1, Theorem 4.1, and Theorem 5.1.

6. Conclusion

The asymptotic traffic flow in a Poissonian city has been represented as the 4-volume of a stochastic geometric object in [7], but the object itself (an unbounded region in $\mathbb{R}^4$) is somewhat intransigent. The above work shows how to represent the volume in terms of integrals involving the strictly monotonic continuous concave seminal curves $\Gamma_\pm$, and, furthermore, establishes approximations which supply the theory necessary to approximate and effectively simulate the 4-volume with explicit L^1 error.

Work for a future occasion includes investigation of the amount of computational effort required to achieve stage-N approximations corresponding to (3.7). This is a nontrivial task, since account must be taken of the effort required to approximate each of the $C_n^{\pm}$ for $n = 0, 1, \ldots, N$.

It is natural then to ask whether it might be possible to translate this work into the construction of a perfect simulation algorithm. For example, Møller's nearly perfect simulation algorithm for conditionally specified models [9] (simulating to within floating point error) was improved by Wilson to an efficient and exactly perfect simulation algorithm using multishift coupling [12]. Certainly, Fill and Huber [6] have shown how to use dominated coupling from the past to generate exact draws from recursive definitions of perpetuities (see also the work of Blanchet and Sigman [4]); this is suggestive, since the system for $\Gamma'(S_n)$ and S_n ((4.5) and (4.6)) is a similar if more complicated recursive construction. However, in the present case, interest lies in integral quantities derived from (4.5) and (4.6), and it is not obvious how to generate a perfect simulation algorithm from the approximate simulation algorithm implied by the results of Theorem 3.1, Lemma 4.1, Theorem 4.1, and Theorem 5.1. The matter of whether or not such a perfect simulation algorithm exists is left as a significant open question for future work.

References

[1] Aldous, D. J. and Bhamidi, S. (2010). Edge flows in the complete random-lengths network. *Random Structures Algorithms* **37,** 271–311.
[2] Aldous, D. J. and Kendall, W. S. (2008). Short-length routes in low-cost networks via Poisson line patterns. *Adv. Appl. Prob.* **40,** 1–21.
[3] Aldous, D. J., McDiarmid, C. and Scott, A. (2009). Uniform multicommodity flow through the complete graph with random edge-capacities. *Operat. Res. Lett.* **37,** 299–302.
[4] Blanchet, J. H. and Sigman, K. (2011). On exact sampling of stochastic perpetuities. In *New Frontiers in Applied Probability* (J. Appl. Prob. Spec. Vol. **48A**), eds P. Glynn, T. Mikosch and T. Rolski, Applied Probability Trust, Sheffield, pp. 165–182.
[5] Chiu, S. N., Stoyan, D., Kendall, W. S. and Mecke, J. (2013). *Stochastic Geometry and Its Applications*. John Wiley, Chichester.
[6] Fill, J. A. and Huber, M. L. (2010). Perfect simulation of Vervaat perpetuities. *Electron. J. Prob.* **15,** 96–109.
[7] Kendall, W. S. (2011). Geodesics and flows in a Poissonian city. *Ann. Appl. Prob.* **21,** 801–842.
[8] Meyn, S. P. and Tweedie, R. L. (1993). *Markov Chains and Stochastic Stability*. Springer, London.

[9] Møller, J. (1999). Perfect simulation of conditionally specified models. *J. R. Statist. Soc. B* **61,** 251–264.
[10] Roberts, G. O. and Tweedie, R. L. (1996). Geometric convergence and central limit theorems for multidimensional Hastings and Metropolis algorithms. *Biometrika* **83,** 95–110.
[11] Vervaat, W. (1979). On a stochastic difference equation and a representation of nonnegative infinitely divisible random variables. *Adv. Appl. Prob.* **11,** 750–783.
[12] Wilson, D. B. (2000). Layered multishift coupling for use in perfect sampling algorithms (with a primer on CFTP). In *Monte Carlo Methods* (Fields Inst. Commun. **26**; Toronto, Ontario, 1998), ed. N. Madras, American Mathematical Society, Providence, RI, pp. 143–179.

WILFRID S. KENDALL, *University of Warwick*
Department of Statistics, University of Warwick, Coventry CV5 6FQ, UK.

https://doi.org/10.1239/jap/1417528482 Published online by Cambridge University Press